

Preparation and Catalytic Activities of Au/Co Bimetallic Nanoparticles for Hydrogen Generation from NaBH₄ Solution

Xiaofeng Wang¹, Zili Huang¹, Lilin Lu², Haijun Zhang^{3,4,*}, Yingnan Cao^{3,4},
Yajun Gu^{3,4}, Zhong Cheng⁵, and Shaowei Zhang⁴

¹Hubei Key Laboratory for Efficient Utilization and Agglomeration of Metallurgical Mineral Resources, Wuhan University of Science and Technology, Wuhan 430081, China

²College of Chemical Engineering and Technology, Wuhan University of Science and Technology, Wuhan 430081, China

³College of Materials and Metallurgy, Wuhan University of Science and Technology, Wuhan, Hubei Province 430081, China

⁴State Key Laboratory Breeding Base of Refractories and Ceramics, Wuhan University of Science and Technology, Wuhan 430081, China

⁵College of Chemistry and Molecular Sciences, Wuhan University, Wuhan 430072, China

A series of poly(*N*-vinyl-2-pyrrolidone)-protected Au/Co bimetallic nanoparticles (BNPs) were prepared by a simple route based on dropwise addition of NaBH₄. Their structures, particle sizes, and chemical compositions were characterized by Ultraviolet-visible spectrophotometry, X-ray photoelectron spectroscopy, Transmission electron microscopy and High-resolution transmission electron microscopy, and their catalytic activity for the hydrogen generation from hydrolysis of an alkaline NaBH₄ solution was examined. As-prepared alloy-structured Au/Co BNPs had an average size between 2.8 and 3.6 nm and showed a higher catalytic activity for the hydrogen generation than the corresponding Au and Co monometallic nanoparticles (MNPs). Of all the MNPs and BNPs, Au₂₀Co₈₀ BNPs exhibited the highest catalytic activity, and a hydrogen generation rate of 480 mol-H₂·h⁻¹·mol-M⁻¹ was achieved. The high catalytic activity of the BNPs can be ascribed to the formation of negatively charged Au atoms and positively charged Co atoms as a result of the electronic charge transfer effects in the BNPs.

Keywords: Au/Co, Bimetallic Nanoparticles, Catalytic Activity, Hydrogen Generation, NaBH₄, Hydrolysis.

1. INTRODUCTION

Hydrogen (H₂) is a globally accepted clean fuel.^{1,2} Recently, much attention has been paid to the hydrolysis of chemical hydrides (NaBH₄, KBH₄, LiBH₄, etc.),^{3–8} which as a hydrogen source shows a number of advantages in portable applications, including, nonflammability and stability in air, easy control of hydrogen generation rate, recyclability of the side products, and a high H₂ storage capacity. Among these chemical hydrides, sodium borohydride (NaBH₄) is the most feasible for safe and practical production of hydrogen for fuel cells.⁹ It hydrolyzes in

the presence of a suitable catalyst, releasing hydrogen gas along with the formation of water-soluble sodium metaborate, NaBO₂.

Some non-noble transition metals, in particular, Co, were reported to exhibit good activities for hydrogen generation from NaBH₄.^{10,11} For example, hydrogen could be released from an aqueous solution of NaBH₄ within 2.5 min (molar ratio of Co/NaBH₄ = 0.0056) when a fluorinated cobalt was as a catalyst.¹² A Co–B thin film catalyst prepared by the pulsed laser deposition technique was about 2.5 times more efficient in hydrogen generation than a Co powder catalyst.¹³ The activity of a Cr-doped Co–B powder catalyst was about 4 times higher than that

*Author to whom correspondence should be addressed.

of a pure Co–B catalyst in hydrogen generation from the NaBH₄ hydrolysis.¹⁴

Gold (Au)^{15,16} has long been known to be catalytically less active than other transition metals. However, its nanoparticles supported on metal oxides such as TiO₂ exhibited an extraordinary high activity for low-temperature catalytic combustion, partial oxidation of hydrocarbons, hydrogenation of unsaturated hydrocarbons, and reduction of nitrogen oxides.¹⁷ Currently, a great deal of attention is being paid to gold-containing bimetallic nanoparticle (BNP) catalysts because of their high catalytic activities at low-temperatures for a series of important reactions,^{18,19} such as oxidation of CO and H₂,^{20,21} reduction of NO_x,²² epoxidation of C₃H₆,²³ selective glucose oxidation^{24–25} and combustion of methane.²⁶ Nevertheless, to our knowledge, there has been no reported work on the catalytic activity of Au-containing BNPs for hydrogen generation from NaBH₄.

In the present work, Au/Co BNPs were synthesized and characterized and their catalytic activities for hydrogen generation from the hydrolysis of an alkaline NaBH₄ solution examined in detail. In addition, density functional theory (DFT) calculations were carried out, assisting understanding the catalytic effects of Au/Co BNPs. The results showed that the negatively charged Au atoms due to electron donation from the neighboring Co atoms in the Au/Co BNPs had acted as catalytically active sites for the hydrogen generation from the hydrolysis of an alkaline NaBH₄ solution, and the presence of the negatively charged Au atoms was also supported by X-ray photoelectron spectroscopy (XPS) examinations and the DFT calculations.

2. EXPERIMENTAL DETAILS

2.1. Raw Materials

Hydrogen tetrachloroaurate (III) tetrahydrate (HAuCl₄ · 4H₂O, 99.9%), cobalt (II) chloride hexahydrate (CoCl₂ · 6H₂O, 99%), sodium borohydride (NaBH₄, 96.0%), poly(*N*-vinyl-2-pyrrolidone) (PVP, K30, average molecular-weight of about 30,000), and sodium hydroxide (NaOH, 96.0%) purchased from Sinopharm Ltd., were used directly as the main starting materials without further purification. All glassware and Teflon-coated magnetic stirring bars were cleaned with aqua regia, followed by repeated rinsing with pure water.

2.2. Preparation of PVP-Protected Au/Co BNPs

A series of Au/Co BNPs stabilized by PVP were prepared by dropwise addition of NaBH₄. For example, Au₂₀Co₈₀ BNPs (Hereafter, the subscripts indicate the synthetic feeding ratio of the two metals) were prepared as follows: aqueous solutions of HAuCl₄ · 4H₂O (10 mL, 0.66 mM) and CoCl₂ · 6H₂O (40 mL, 0.66 mM) were combined with an aqueous PVP solution (50 mL, 66 mM in monomer unit; *R*_{PVP} is defined as the molar ratio of PVP in monomer

units to the total metal ions) in a 250 mL two-neck flask and then stirred at 0 °C for 30 min. After that, an aqueous solution of NaBH₄ (10 mL, 16.5 mM, 0 °C; *R*_{NaBH₄} is defined as the molar ratio of NaBH₄ to the total metal ions) was added at a rate of one drop in every three seconds under vigorous stirring for about 10 min, and then the solutions were stirred for another 1 h at 0 °C.

2.3. Characterization of Nanoparticles

Ultraviolet and visible light (UV-Vis) absorption spectra were recorded over 200–800 nm with a Shimadzu 2550 recording spectrophotometer using a quartz cell with an optical path length of 10 mm. Transmission electron microscopy (TEM) images were taken at the accelerated voltage of 80 kV using an FEI Tecnai G² 50-S-TWIN TEM. The specimens were obtained by dropping one or two droplets of the Au/Co colloidal ethanol solution onto a copper microgrid covered with a thin amorphous carbon film and followed by evaporating the ethanol in air at room temperature. For each sample, generally at least 200 particles from different parts of the grid were selected to evaluate their mean diameter and size distribution. High-resolution TEM (HR-TEM) images were taken at the accelerated voltage of 200 kV using a JEM-2100F Field Emission High-resolution TEM. XPS measurement was performed using a Quantum 2000 spectrometer with Al K α radiation. Binding energies (BE) were normalized by the C(1s) BE of adventitious carbon contamination taken as 284.6 eV, and the analyses of Au were based on Au4f_{5/2} and Au4f_{7/2} peaks.

2.4. Catalytic Activity of Au/Co BNPs for the Hydrolysis of Alkaline NaBH₄

The catalytic activity of Au/Co BNPs was evaluated based on the volume of hydrogen gas generated from hydrolysis of an alkaline NaBH₄ solution. Experiment was carried out in a two-necked round-bottom flask with one opening connected to a gas burette and the other to an addition funnel with a pressure-equalization arm. In all tests, the reaction was started by vigorous stirring the mixture of Au/Co BNP catalyst and the alkaline NaBH₄ solution (50 mL, 30 mM and pH 12.) in the molar ratio of 0.05. The temperature for activity evolution was maintained at 30 °C using a water bath, and the volume of the generated hydrogen gas was measured by the displacement level of water in a burette.

2.5. Density Functional Theory (DFT) Calculation

Electronic structures of the M₅₅ clusters were calculated using the Amsterdam Density Functional (ADF) program package developed by Baerends and coworkers. In these calculations, the Triple- ζ plus Polarization basis (TZP) sets and the relativistic effects with Zero Order Regular Approximation (ZORA) were employed for all the elements. The exchange-correlation energy of electrons was described in the generalized gradient approximation

(GGA) with the functional parameterization of PBE. The criterion of the self-consistent convergence of total energy was set as ≥ 0.001 eV/atom. The atomic charges were taken from the Multipole Derived Charge analysis (MDC-q).

3. RESULTS AND DISCUSSION

To examine the effect of compositions of Au/Co BNPs on their catalytic activities, a series of BNPs with various atomic ratios of Au/Co were prepared using dropwise addition of NaBH₄. It is well known that UV-Vis absorption spectra are strongly dependant on the size, composition and dielectric properties of nanoparticles as well as their local environment. Figure 1 shows UV-Vis spectra of Au/Co BNP aqueous dispersions with various compositions. The spectrum of Au NP aqueous dispersion exhibits a plasmon absorbance peak around 520 nm, which is consistent with the result previously reported,²⁷ whereas the spectrum of Co NP aqueous dispersion exhibits a featureless and monotonically increasing absorbance toward the high energy range. The UV-Vis spectra in Figure 1 also show the suppression of the Au plasmon peaks with increasing the Co content, which suggests the co-existence of Co atoms and Au atoms on the surfaces of Au/Co BNPs. When the molar ratio of Au/Co is 20/80, the 520-nm surface plasmon peak from the Au atoms finally disappears, indicating the presence of many Co atoms on the surfaces of the BNPs. The UV-Vis spectra exclude the existence of Co_{core}/Au_{shell} BNPs and Au_{core}/Co_{shell} BNPs in the present Au/Co BNPs. The reasons are as follows. If the former were formed, there would be a plasmon band observed at about 520 nm for all the BNPs due to the Au surface plasmon resonance. On the other hand, if the latter (i.e., Co deposited onto Au NPs) were present, there would be no plasmon resonance peaks observed in the UV-Vis spectra of all the BNPs.

Figure 2 presents a representative set of TEM images and size distribution histograms of as-prepared Au/Co

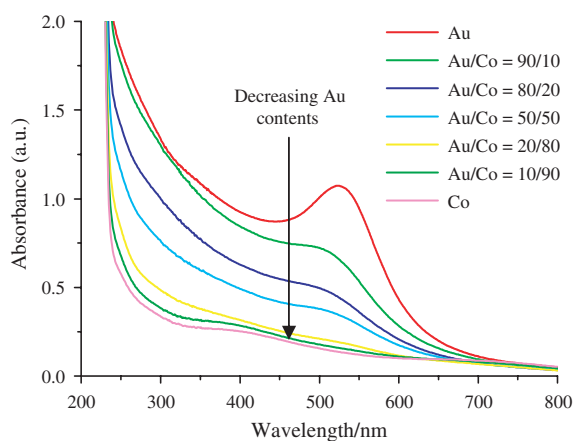


Figure 1. UV-Vis spectra of colloidal dispersions of Au and Co MNPs, Au/Co BNPs with various contents of Co.

BNPs with various compositions. The size distribution analysis based on the TEM images gives the average diameter of 3.0 ± 1.3 nm for Au, 3.1 ± 1.1 nm for Au₉₀Co₁₀, 3.0 ± 0.9 nm for Au₈₀Co₂₀, 2.8 ± 1.1 nm for Au₅₀Co₅₀, 3.6 ± 0.9 nm for Au₂₀Co₈₀, and 3.0 ± 1.0 nm for Au₁₀Co₉₀ NPs. All the NPs were spherical and well-isolated, with a standard deviation of about 30% in the diameter. In the case of Co MNPs, large average diameters up to several tens nanometers were determined based on TEM (not shown). It can be deduced that as-prepared Au/Co nanoparticles were composed of the bimetallic nanoparticles based on the following reasons: (1) large particles up to tens nanometers seen in the case of Co NPs were not present in the as-prepared Au/Co bimetallic samples, and (2) the particle size distribution of Au/Co BNPs was much narrower than that of the physical mixture of Au and Co MNPs.

In order to further confirm the formation of alloyed structures in the as-prepared Au/Co BNPs, lattice fringes analysis based on HR-TEM images of the Au₂₀Co₈₀ colloidal dispersions was also carried out. As revealed by Figure 3, the particles possessed crystalline structures. The interplanar distances of four individual randomly-chosen particles were measured as 0.218 nm (particle-1), 0.194 nm (particle-2), 0.232 nm (particle-3), and 0.231 nm (particle-4), respectively, as labeled in Figure 3. These lattice fringes do not match with any reflection plane distances of pure Au or Co shown in Table I, which rules out the formation of individual Au and Co NPs in the as-prepared Au/Co nanoparticles. Nevertheless, it should be noted that the interplanar distances of 0.218 nm, 0.232 nm and 0.231 nm, lie between the interplanar spacing of Co (111) (0.205 nm) and that of Au (111) (0.236 nm), suggesting that an alloyed structure was formed in the particles and the interplanar spacing can be assigned to the (111) plane of the alloy-structured Au/Co. Similarly, the interplanar distances, 0.194 nm, observed from particle-2, can be assigned to the (200) plane of the alloy-structured Au/Co (Table II). Moreover, it should be pointed that, except particle 1, the measured interplanar distances are not in consistent with the theoretical values of bulk Au₂₀Co₈₀ alloy as listed in Table II. This result and the various interplanar distances of the (111) plane observed from different particles indicate that the as-prepared Au₂₀Co₈₀ alloy BNPs did not possess an even composition. In other words, not all of the as-prepared individual Au₂₀Co₈₀ BNPs have the chemical composition of Au/Co = 20/80. In a word, based on the results of UV-Vis, TEM images and lattice spacing of HR-TEM images, it can be reasonably deduced that alloy-structured Au/Co BNPs were formed.

The catalytic properties of as-prepared Au/Co BNPs were studied using the hydrogen generation from hydrolysis of an alkaline NaBH₄ solution as a working tool. The activity varies with the composition of the Au/Co BNPs

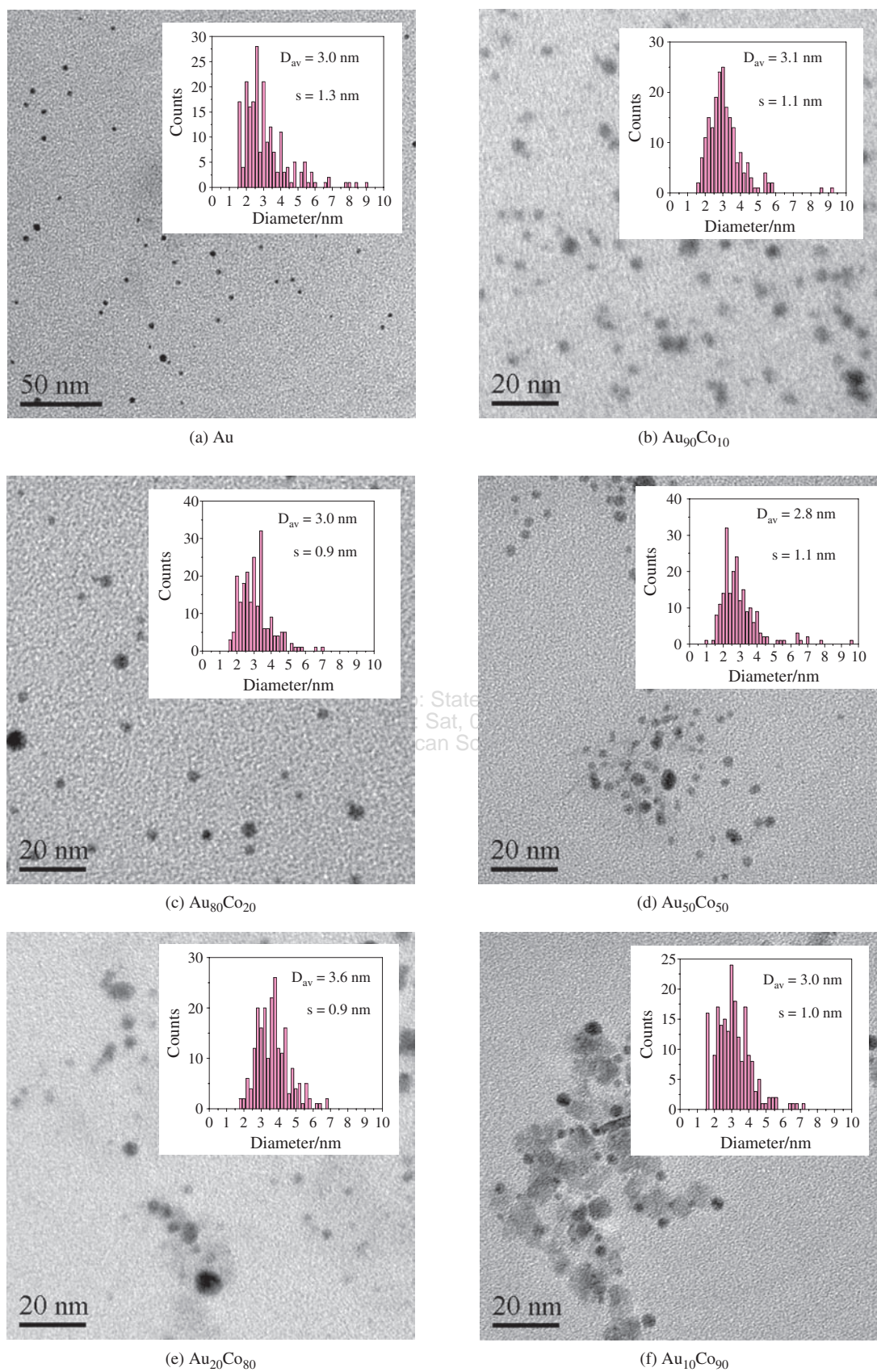


Figure 2. TEM micrographs and size distribution histograms of Au, Au₉₀Co₁₀, Au₈₀Co₂₀, Au₅₀Co₅₀, Au₂₀Co₈₀ and Au₁₀Co₉₀ nanoparticles.

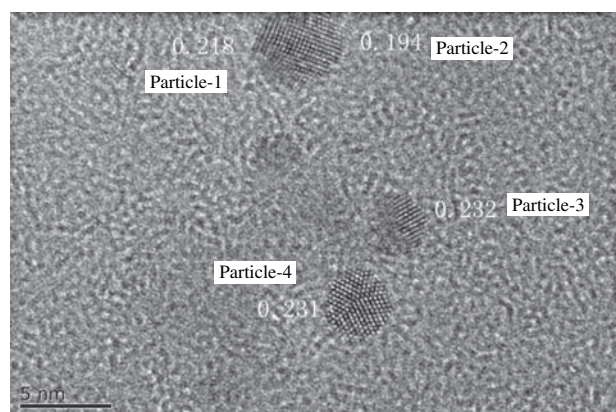


Figure 3. HR-TEM image of as-prepared Au₂₀Co₈₀ BNPs.

as shown in Figure 4. All the BNPs showed a higher catalytic activity than pure Au or Co MNPs. The highest catalytic activity, 480 mol-H₂ · h⁻¹ · mol-M⁻¹, was achieved in the case of Au₂₀Co₈₀ BNPs. It is more than 3.5 times higher than that of Au or Co BNPs (130 and 77 mol-H₂ · h⁻¹ · mol-M⁻¹, respectively for Au and Co MNPs). Even the activities for hydrogen generation of the prepared Au/Co BNPs were normalized by the specific surface areas, the Au₂₀Co₈₀ BNPs still show the highest activity (results not shown here). The higher catalytic activity of the Au/Co BNPs than that of MNPs is attributable to the effects of electronic charge transfer between the Au and Co atoms. Such effects were considered previously to be

Table I. Theoretical lattice spacing of bulk Au and Co with various reflection planes.

Reflection planes	Lattice distances, nm	
	Au	Co
(111)	0.236	0.205
(200)	0.204	0.177
(220)	0.144	0.120
(311)	0.123	0.107
(222)	0.118	0.102

Notes: (Au: JCPDS 89-3697; Co: JCPDS 15-0806).

Table II. Lattice spacing and indexed reflection planes of Au₂₀Co₈₀ BNPs determined by HR-TEM.

Au ₂₀ Co ₈₀ BNPs	Measured lattice distances (nm)		Indexed reflection planes of Au/Co alloy BNPs	Theoretical lattice distance of bulk Au ₂₀ Co ₈₀ alloy ²⁸
	Remarks			
Particle-1	0.218	In the range of Au(111) and Co(111)	(111)	0.212 nm for (111) plane*
Particle-2	0.194	In the range of Au(200) and Co(200)	(200)	0.184 nm for (200) plane*
Particle-3	0.232	In the range of Au(111) and Co(111)	(111)	0.212 nm for (111) plane*
Particle-4	0.231	In the range of Au(111) and Co(111)	(111)	0.212 nm for (111) plane*

Notes: *Calculated based on the lattice parameters of Au₂₀Co₈₀ alloy.

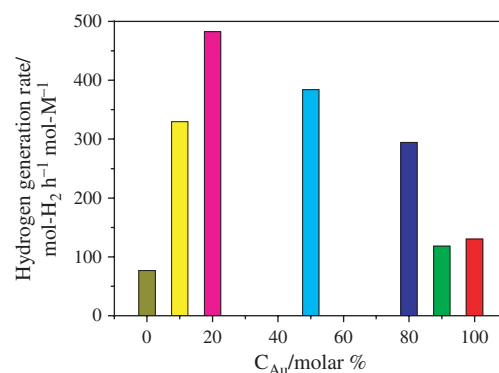


Figure 4. Effect of chemical composition on hydrogen generation from the hydrolysis of alkaline NaBH₄ solution over as-prepared Au/Co BNPs.

responsible for the high catalytic activities of several types of BNPs.^{29,30} In the case of the Au/Co BNPs, the ionization potentials of Au and Co are 9.22 and 7.86 eV, respectively. The electronic charges could transfer from Co atoms to Au atoms, leading to an increase in the electron density on the Au atoms. Consequently, the negatively charged Au atoms and positively charged Co atoms could act as catalytically active sites for hydrogen generation from the hydrolysis of an alkaline NaBH₄ solution.

To prove the electronic charge transfer effects and the presence of the negatively charged Au atoms and positively charged Co atoms in the BNPs, the electronic properties of the Au/Co BNPs were initially investigated using XPS. PVP-protected Au₂₀Co₈₀ BNPs prepared with a low content of PVP ($R_{\text{PVP}} = 5$) were examined by high-resolution XPS using monochromated Al K α electron radiation. As shown in Figure 5, the electron apparent BEs of Au4f_{5/2} and Au4f_{7/2} in the Au₂₀Co₈₀ BNPs were 87.05 eV and 83.19 eV, respectively. The electron apparent BE of Au4f_{5/2} was about 0.58 eV lower than that of bulk Au4f_{5/2} (87.63 eV), and a similar result was also observed for Au4f_{7/2} (about 0.76 eV lower than that of bulk Au4f_{7/2} of 83.95 eV). The negative shifts of the Au4f_{5/2} and Au4f_{7/2}

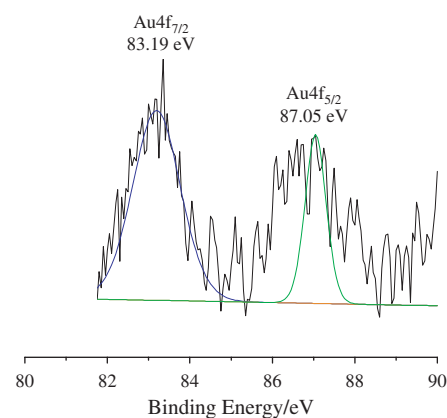


Figure 5. Au XPS core level spectrum recorded from Au₂₀Co₈₀ BNPs synthesized with a low content of PVP ($R_{\text{PVP}} = 5$).

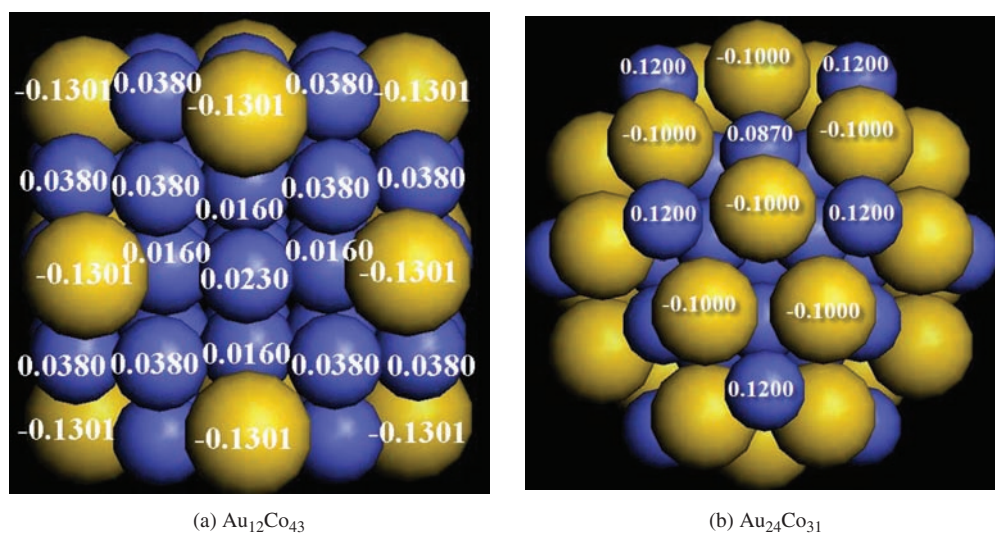


Figure 6. DFT calculations of electronic structures of Au₁₂Co₄₃ and Au₂₄Co₃₁ BNPs (yellow, Au; and blue, Co).

suggest that the Au atoms in the BNPs were indeed negatively charged, and the Co atoms did donate electrons to the Au atoms.

To further confirm the electron donation from Co atoms to Au atoms, DFT calculations of a M₅₅ model NPs of Au₁₂Co₄₃ and Au₂₄Co₃₁ (the subscripts stand for the number of atoms in the BNPs) were performed to assist understanding the electronic states of Co and Au atoms in the BNPs (Fig. 6). The most important finding from these calculations is that Au atoms are indeed negatively charged, whereas the Co atoms positively charged due to the electronic charge transfer from them to Au atoms. The DFT calculation results are consistent with those of XPS, and both confirm the presence of the electronic charge transfer effect in the BNPs. It is considered that both the negatively charged Au atoms and positively charged Co atoms acted as catalytic active sites for hydrogen generation from hydrolysis of NaBH₄. The possible electronic charge transfer effects in Au/Co BNPs are illustrated in Figure 7. At this stage, the detailed catalytic mechanism of the BNPs for hydrogen generation from hydrolysis of NaBH₄ is still not very clear, work along this line is now in progress. In the presence of catalysts, NaBH₄ can generate hydrogen rapidly in the following way:

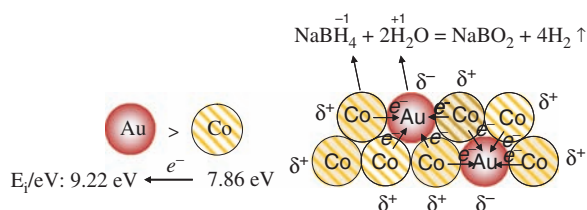
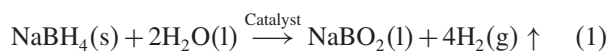


Figure 7. Schematic illustration of electronic charge transfer effects in Au₂₀Co₈₀ BNPs (E_i : Ionization energy).

and a plausible mechanism involving adsorption of BH₄⁻ onto the NPs to form an activated complex which might be the rate-determining step, followed by H₂ production through attack by a H₂O molecule can be used to describe the process. In the case of catalysis by the present BNPs, the positive charged Co atoms may favor the absorption of BH₄⁻, and the negatively charged Au atoms would transfer electrons to the molecular H₂O to generate hydrogen. Thus, we predict that the enhancement of the catalytic activity for hydrogen production from NaBH₄ by present Au/Co BNPs is due to the synergetic effect between the charged atoms and BH₄⁻/H₂O, even though we have no strict evidence on it.

4. CONCLUSIONS

A series of Au/Co alloy BNPs with average sizes of 2.8–3.6 nm were prepared by dropwise addition of NaBH₄. The as-prepared Au/Co BNPs showed higher catalytic activities for hydrolysis of NaBH₄ than corresponding Au and Co MNPs, which could be ascribed to the presence of negatively charged Au atoms and positively charged Co atoms. The catalytic activity of Au₂₀Co₈₀ BNPs for hydrogen generation from the hydrolysis of an alkaline NaBH₄ solution is 480 mol-H₂·h⁻¹·mol-M⁻¹ under the conditions of pH = 12 and 30 °C.

Acknowledgments: This work was financially supported by National Natural Science Foundation of China (General program, 51272188).

References and Notes

1. P. Chen, Z. Xiong, J. Luo, J. Lin, and K. L. Tan, *Nature* **420**, 302 (2002).
2. J. M. Yan, X. B. Zhang, S. Han, H. Shioyama, and Q. Xu, *Inorg. Chem.* **48**, 7389 (2009).

3. S. C. Amendola, S. L. Sharp-Goldman, M. S. Janjua, N. C. Spencer, M. T. Kelly, P. J. Petillo, and M. Binder, *Int. J. Hydrogen Ener.* 25, 969 (2000).
4. Y. Kojima, K. I. Suzuki, K. Fukumoto, M. Sasaki, T. Yamamoto, Y. Kawai, and H. Hayashi, *Int. J. Hydrogen Ener.* 27, 1029 (2002).
5. H. I. Schlesinger, H. C. Brown, A. E. Finholt, J. R. Gilbreath, H. R. Hoekstra, and E. K. Hyde, *J. Am. Chem. Soc.* 75, 215 (1953).
6. S. C. Amendola, S. L. Sharp-Goldman, M. S. Janjua, M. T. Kelly, P. J. Petillo, and M. Binder, *J. Power Sources* 85, 186 (2000).
7. Y. Kojima, Y. Kawai, M. Kimbara, H. Nakanishi, and S. Matsumoto, *Int. J. Hydrogen Ener.* 29, 1213 (2004).
8. M. Chandra and Q. Xu, *J. Power Sources* 159, 855 (2006).
9. S. Özkır and M. Zahmakıran, *J. Alloys Compd.* 404–406, 728 (2005).
10. J. Lee, K. Y. Kong, C. R. Jung, E. Cho, S. P. Yoon, J. Han, T. G. Lee, and S. W. Nam, *Catal. Today* 120, 305 (2007).
11. M. Rakap and S. Özkır, *Appl. Catal. B* 91, 21 (2009).
12. S. Suda, Y. M. Sun, B. H. Liu, Y. Zhou, S. Morimitsu, K. Arai, N. Tsukamoto, M. Uchida, Y. Candra, and Z. P. Li, *Appl. Phys. A* 72, 209 (2001).
13. N. Patel, G. Guella, A. Kale, A. Miotello, B. Patton, C. Zanchetta, L. Mirengi, and P. Rotolo, *Appl. Catal. A* 323, 18 (2007).
14. R. Fernandes, N. Patel, and A. Miotello, *Appl. Catal. B* 92, 68 (2009).
15. J. J. Niu, V. Presser, C. J. Karwacki, and Y. Gogotsi, *Mater. Express* 1, 259 (2011).
16. R. Nirmala, H. M. Park, D. Kalpana, H. S. Kang, R. Navamathavan, Y. S. Lee, and H. Y. Kim, *J. Biomed. Nanotechnol.* 7, 342 (2011).
17. M. Haruta, *Catal. Today* 36, 153 (1997).
18. M. Shkir, S. Aarya, R. Singh, M. Arora, G. Bhagavannarayana, and T. D. Senguttuvan, *Nanosci. Nanotechnol. Lett.* 4, 405 (2012).
19. X. J. Bai, T. Cao, and C. B. Cao, *Sci. Adv. Mater.* 4, 1007 (2012).
20. H. Huber, D. McIntosh, and G. A. Ozin, *Inorg. Chem.* 16, 975 (1977).
21. M. Haruta, N. Yamada, T. Kobayashi, and S. Iijima, *J. Catal.* 115, 301 (1989).
22. A. Ueda and M. Haruta, *Gold Bull.* 32, 3 (1999).
23. B. S. Uphade, Y. Yamada, T. Akita, T. Nakamura, and M. Haruta, *Appl. Catal. A* 215, 137 (2001).
24. H. J. Zhang and N. Toshima, *Catal. Sci. Technol.* 3, 268 (2013).
25. N. Toshima and H. J. Zhang, *Macromol. Symp.* 317–318, 149 (2012).
26. R. J. H. Grisel, P. J. Kooyman, and B. E. Nieuwenhuys, *J. Catal.* 191, 430 (2000).
27. H. Tsunoyama, N. Ichikuni, H. Sakurai, and T. Tsukuda, *J. Am. Chem. Soc.* 131, 7086 (2009).
28. H. Okamoto, T. B. Massatski, M. Hasebe, and T. Nishizawa, *Bulletin of Alloy Phase Diagram* 6, 449 (1985).
29. H. J. Zhang and N. Toshima, *Appl. Catal. A* 447–448, 81 (2012).
30. G. W. Zhan, J. L. Huang, M. M. Du, I. Abdul-Rauf, Y. Ma, and Q. B. Li, *Mater. Lett.* 65, 2990 (2011).

Received: 21 September 2013. Accepted: 4 November 2013.

Delivered by Publishing Technology to: State University of New York at Binghamton
IP: 128.226.37.5 On: Sat, 06 Dec 2014 14:03:50
Copyright: American Scientific Publishers